Integration of Satellite Soil Moisture and Rainfall Observations over the Italian Territory

LUCA CIABATTA, LUCA BROCCA, CHRISTIAN MASSARI, AND TOMMASO MORAMARCO

Research Institute for Geo-Hydrological Protection, National Research Council, Perugia, Italy

SILVIA PUCA AND ANGELO RINOLLO

National Civil Protection Department, Rome, Italy

SIMONE GABELLANI

International Centre on Environmental Monitoring, Savona, Italy

WOLFGANG WAGNER

Department of Geodesy and Geoinformation, Vienna University of Technology, Vienna, Austria

(Manuscript received 4 June 2014, in final form 6 February 2015)

ABSTRACT

State-of-the-art rainfall products obtained by satellites are often the only way of measuring rainfall in remote areas of the world. However, it is well known that they may fail in properly reproducing the amount of precipitation reaching the ground, which is of paramount importance for hydrological applications. To address this issue, an integration between satellite rainfall and soil moisture SM products is proposed here by using an algorithm, SM2RAIN, which estimates rainfall from SM observations. A nudging scheme is used for integrating SM-derived and state-of-the-art rainfall products. Two satellite rainfall products are considered: H05 provided by EUMESAT and the real-time (3B42-RT) TMPA product provided by NASA. The rainfall dataset obtained through SM2RAIN, $SM2R_{ASC}$, considers SM retrievals from the Advanced Scatterometer (ASCAT). The rainfall datasets are compared with quality-checked daily rainfall observations throughout the Italian territory in the period 2010–13. In the validation period 2012–13, the integrated products show improved performances in terms of correlation with an increase in median values, for 5-day rainfall accumulations, of 26% (18%) when $SM2R_{ASC}$ is integrated with the H05 (3B42-RT) product. Also, the median root-mean-square error of the integrated products is reduced by 18% and 17% with respect to H05 and 3B42-RT, respectively. The integration of the products is found to improve the threat score for medium–high rainfall accumulations. Since $SM2R_{ASC}$, H05, and 3B42-RT datasets are provided in near–real time, their integration might provide more reliable rainfall products for operational applications, for example, for flood and landslide early warning systems.

1. Introduction

Obtaining accurate rainfall estimates is of paramount importance, as rainfall plays a key role in many fields, such as natural hazard assessment, drought management, weather forecasting, agriculture, and disease prevention (Dinku et al. 2007). The use of ground-monitoring rain gauge stations is affected by uncertainties due to, for instance, the limited spatial representativeness of sensors (Kidd et al. 2012) and the not always sufficient density of measuring networks (Rudolf and Schneider 2005). Satellite rainfall products can be used to overcome these issues and, currently, are the main, if not only, source of information over many areas of the world (Kidd and Levizzani 2011). However, satellite products occasionally fail in reproducing the long-term and single-event rainfall patterns because of the indirect nature of satellite observation (Kucera et al. 2013).

Corresponding author address: Luca Ciabatta, Research Institute for Geo-Hydrological Protection, National Research Council, Via Madonna Alta 126, 06128 Perugia, Italy.
E-mail: luca.ciabatta@irpi.cnr.it

DOI: 10.1175/JHM-D-14-0108.1

With the purpose of improving the accuracy of satellite rainfall products, three approaches using satellite soil moisture SM data were recently developed (Crow et al. 2009; Pellarin et al. 2013; Brocca et al. 2013). In the first approach, Crow et al. (2009) assimilated Advanced Microwave Scanning Radiometer for Earth Observing System (AMSR-E; Jackson et al. 2007) SM data into an antecedent precipitation index (API) model, in order to correct the 2–10 day rainfall accumulation in a data assimilation framework. In the second approach, Pellarin et al. (2013) coupled an API model with a microwave emission model to simulate brightness temperature TB. Then, the satellite-based rainfall product estimates are modulated, with a multiplicative factor, in order to minimize the difference between the modeled and the AMSR-E-derived TB. Recently, Brocca et al. (2013) proposed a method for estimating rainfall using satellite SM observations, called SM2RAIN. The method is based on the inversion of the soil water balance equation. That is, it estimates the rainfall by using the change in time of the amount of water stored into the soil, thus considering it as a natural rain gauge. In practice, SM data are not used to correct rainfall, as in Crow et al. (2009) and Pellarin et al. (2013), but to directly estimate rainfall. SM2RAIN has been applied at both local (Brocca et al. 2013) and global scales (Brocca et al. 2014) with ground and satellite SM data as input. The satisfactory results obtained in these studies prove the SM2RAIN's capability of estimating rainfall.

On this basis, a method to integrate satellite rainfall datasets and SM2RAIN-derived rainfall data over the Italian territory is presented here. The SM2RAIN method is applied to the satellite SM product obtained by the Advanced Scatterometer (ASCAT) on board the MetOp satellites (Wagner et al. 2013). Because of the temporal resolution of satellite SM data, the method is applied at daily time steps. Two satellite rainfall products are used in this analysis: H05 provided by the European Organisation for the Exploitation of Meteorological Satellites (EUMETSAT) Satellite Application Facility on Support to Operational Hydrology and Water Management (H-SAF; http://hsaf.meteoam.it/) project (Mugnai et al. 2013; Puca et al. 2014); and the Tropical Rainfall Measuring Mission (TRMM) Multisatellite Precipitation Analysis (TMPA), version 7, delivered in real time, 3B42-RT (http://trmm.gsfc.nasa.gov; Huffman et al. 2007).

The purpose of this study is twofold. First, the performance of different satellite-based rainfall products is assessed over the Italian territory. Specifically, their capability to estimate 1- and 5-day rainfall accumulations over an extended period (4 years) is assessed mainly for their application to hydrological and early warning systems. To this end, it is worth noting that this is the first attempt to carry out a validation of the recently delivered H05 satellite rainfall product over a long time period.

The second purpose is to investigate the increase in accuracy that can be obtained in precipitation estimates from the integration of an SM-derived rainfall product into state-of-the-art rainfall products, thus allowing us to improve the reliability of satellite products in a context of hydrological framework.

The analyzed products are compared with a rainfall observation dataset obtained from the interpolation of ~3000 rain gauges throughout the Italian territory. The comparison is performed by considering a calibration and a validation period and by computing continuous and categorical metrics. The assessment of the performance scores is carried out by considering their spatial, temporal (on monthly scale), and seasonal variations, in order to fully characterize the accuracy of each product and the benefits obtained from the integration of rainfall and SM data.

2. Datasets

Four rainfall datasets (three from satellite data and one from rain gauge data) and one satellite SM dataset, characterized by different temporal and spatial resolutions, are considered in the period from 1 January 2010 to 31 December 2013. To match the different temporal and spatial resolutions of the different products, each of them is remapped (through the nearest-neighbor algorithm) over a regular grid with spacing of 12.5 km (2043 grid points in total for the Italian territory). The selected spacing is a compromise between the native grids of the different satellite products, and it is found to not significantly affect the results (e.g., percentage change in the correlation coefficient R is less than 7%). Concerning the remapping methodology, different techniques have been used at the beginning of this study (nearest neighbor, inverse distance weighted, and kriging), and we found that the nearest-neighbor method provides satisfactory results in a very short computational time. The cumulated daily rainfall between 0000 and 2400 UTC + 1 h(i.e., local time) is computed for each rainfall product, while the SM data are interpolated in time at 0000 UTC + 1 h in order to match the temporal resolution of the rainfall datasets. A summary of the dataset's spatial and temporal resolutions considered in this study is reported in Table 1.

Satellite rainfall products

The H05 product is provided by EUMETSAT within the H-SAF project. The product is based on frequent precipitation measurements as retrieved by blending

TABLE 1. Spatial and temporal resolution of the analyzed datasets.

Dataset	Spatial resolution	Temporal resolution
Observed rainfall data	12.5 km	Hourly
H05	~5 km	Daily
3B42-RT	0.25° (~25 km)	3 h
$SM2R_{ASC}$	12.5 km	Daily

low-Earth-orbiting (LEO) microwave (MW)-derived precipitation rate measurements and geostationary-Earth-orbiting (GEO) infrared (IR) imagery. This product provides daily rainfall data with a spatial resolution of ~5 km over the H-SAF area (25°–75°N, 25°W–45°E) covering the whole European continent, Iceland, and northern Africa. In a future phase, the area covered by the H-SAF project will be extended through Africa and the South Atlantic Ocean (http://hsaf.meteoam.it/overview.php).

The TMPA 3B42-RT, version 7 (http://trmm.gsfc.nasa.gov), combines rainfall estimates from various satellite sensors. The multisatellite platform uses the TRMM Microwave Imager (TMI), the Special Sensor Microwave Imager (SSM/I) on board the Defense Meteorological Satellite Program (DMSP) satellites, AMSR-E, and the Advanced Microwave Sounding Unit-B (AMSU-B) on board the National Oceanic and Atmospheric Administration (NOAA) satellite series. In addition, the TMPA product also uses GEO IR data, characterized by a higher spatial and temporal resolution than the MW data, through a constellation of GEO satellites. The 3B42-RT product is provided by the National Aeronautics and Space Administration (NASA) with a temporal resolution of 3 h and a spatial resolution of 0.25° for the ±50° north–south latitude band. The cumulated daily rainfall is obtained by simply summing the eight 3-h time windows every day. It should be noted that TMPA data are provided within a time window ±90 min from the nominal time (0000, 0300, . . . , 2100 UTC) while the satellite soil moisture product and the observed rainfall dataset are delivered in local time, that is, UTC + 1. Therefore, the daily cumulated rainfall product from TMPA represents the total rainfall starting, and ending the next day, at 2330 UTC, with only 30 min of delay with respect to the other products. Such a delay can be considered negligible, especially when taking into account the 5 days of accumulated rainfall.

1) GROUND-BASED RAINFALL DATASET

A ground-based rainfall dataset is used as a benchmark in this study. The observed rainfall dataset is obtained by the measurements of more than 3000 rain gauges over the Italian territory spatially interpolated using the Random Generator of Space Interpolations from Uncertain Observations (GRISO; Pignone et al. 2010) algorithm. GRISO is a derivation of the most known kriging method, so it is also based on the geostatistical approach and the use of the semivariogram for generating the spatial structure of the interpolated field. The main innovations are the possibility of using different semivariograms per gauge at the same time and of reducing the computational time with respect to kriging. This dataset provides hourly rainfall observations throughout the Italian territory over a grid with spacing of 12.5 km (Ciabatta et al. 2015). As mentioned previously, the daily product is obtained by summing the hourly data from 0000 to 2400 UTC + 1 h. In this study, observed rainfall data are used as a benchmark because, besides the fact they are used worldwide, they are used operationally by Italian Civil Protection Service for hazard forecast and management; therefore, the satellite rainfall dataset performances are evaluated in such kinds of applications.

2) SATELLITE SOIL MOISTURE DATA

The Surface Soil Moisture (SSM) data are obtained by backscattering retrievals from the ASCAT sensor (C-band scatterometer operating at 5.4 GHz) on board the *MetOp-A* satellite. In this study the Water Retrieval Package (WARP), version 5.51, is used for estimating SM from backscatter measurements. The product has a nearly daily temporal resolution for the study area and a spatial resolution of ~25 km (resampled to 12.5 km; Wagner et al. 2013; http://rs.geo.tuwien.ac.at/products/). Because of the variable temporal resolution of the SSM product, all the SM data have been interpolated in time at 0000 UTC + 1 h each day. This step allows us to compare all the datasets considered in this study in a consistent manner, that is, the daily cumulated rainfall from 0000 to 2400 UTC + 1 h is obtained for each product (see section 3a for the rainfall product obtained from SM data).

3. Methods

a. SM2RAIN

The SM2RAIN method is based on the inversion of the following water balance equation:

$$Znds(t)/dt = p(t) - r(t) - e(t) - g(t), \qquad (1)$$

where Z (L) is the soil depth; n (unitless) is the porosity; $s(t)$ (unitless) is the relative saturation of the soil or relative soil moisture; t (T) is the time; and $p(t)$, $r(t)$, $e(t)$, and $g(t)$ (L T^{-1}) are the precipitation, surface runoff, evapotranspiration, and drainage rates, respectively, where L indicates a unit of length and T indicates a unit of time. According to Famiglietti and Wood (1994), the drainage rate can be expressed using the following equation:

$$g(t) = as(t)^b, \tag{2}$$

where a ($\mathrm{L\,T^{-1}}$) and b are two parameters describing the nonlinearity between the soil saturation and drainage rate (Brocca et al. 2013). By assuming that during rainfall the surface runoff and the evapotranspiration rates are negligible, and by considering $Z^* = Zn$, the rainfall rate is obtained as

$$p(t) \cong Z^* ds(t)/dt + as(t)^b. \tag{3}$$

The Z^*, a, and b parameters are estimated through calibration. The parameter values are calibrated (from 1 January 2010 to 31 December 2011) in a distributed way, defining for each grid point a set of parameters that minimizes the root-mean-square error (RMSE) between observed and simulated 5 days of accumulated rainfall. For a more comprehensive description of the method, the reader is referred to Brocca et al. (2013).

The capability of the SM2RAIN approach to estimate rainfall by using the variation in soil moisture between two different satellite passages represents an important advantage with respect to classical retrieval methods, in terms of estimating the cumulated rainfall value. In the classical satellite-based algorithms (e.g., H05 and 3B42-RT), the instantaneous rainfall rate is estimated at the passages of microwave sensors (radiometers and radars) and then blended between passages by using infrared measurements from GEO satellites. However, if microwave sensors do not pass when it rains, a significant underestimation of rainfall is expected from these algorithms. When using satellite soil moisture data, the amount of rainfall into the soil is recorded, and hence, by computing the difference in the water storage, the cumulated rainfall is estimated. This allows us to keep track of the total rainfall between satellite passages, with a higher degree of accuracy. In this study, the daily cumulated rainfall for SM2RAIN is calculated by considering the difference in SM between 2400 and 0000 UTC + 1 h of each day.

b. Integration technique: Nudging

The integration of the rainfall datasets, obtained by SM2RAIN and the satellite rainfall products (H05 and 3B42-RT), is implemented by using the following nudging scheme (Massari et al. 2014):

$$P_{\mathrm{int}}(t) = P_{\mathrm{sat}}(t) + K[P_{\mathrm{SM2R}}(t) - P_{\mathrm{sat}}(t)], \tag{4}$$

where $P_{\mathrm{int}}(t)$ is the integrated rainfall product; $P_{\mathrm{sat}}(t)$ is the satellite rainfall product; $P_{\mathrm{SM2R}}(t)$ is the SM2RAIN-derived rainfall product; and K is the gain parameter, ranging between 0 and 1. For $K = 0$ there is no integration and only P_{sat} is taken, and for $K = 1$ only the estimated rainfall through the SM2RAIN method is considered. The variable K is calibrated by minimizing the RMSE between observed and integrated rainfall considering 5 days of accumulated rainfall. Two new datasets, integrating the SM2RAIN-derived product using ASCAT as the SM dataset, $\mathrm{SM2R_{ASC}}$, to H05 and 3B42-RT products (hereinafter $\mathrm{SM2R_{ASC}}$+H05 and $\mathrm{SM2R_{ASC}}$+3B42-RT), are obtained. Therefore, the total number of satellite rainfall products analyzed in this study is five: $\mathrm{SM2R_{ASC}}$, H05, 3B42-RT, $\mathrm{SM2R_{ASC}}$+H05, and $\mathrm{SM2R_{ASC}}$+3B42-RT.

c. Performance metrics

To evaluate the performance of the rainfall products, the correlation coefficient and RMSE values over 1 and 5 days of accumulated rainfall are computed separately for each grid point to assess the spatial variability of the products' performance in time. Moreover, the spatial R and RMSE values over 1 and 5 days of accumulated rainfall are computed to assess the products' capability to reproduce the observed rainfall spatial pattern. Also, three categorical metrics are computed, considering the same durations: the probability of detection POD, the false alarm ratio FAR, and the threat score TS. The first refers to the fraction of all correctly predicted events, the second refers to the fraction of predicted events that are actually nonevents, and the third gives integrated information of the overall performance. The three categorical metrics are defined as

$$\mathrm{POD} = \frac{H}{H + M}, \tag{5}$$

$$\mathrm{FAR} = \frac{F}{F + H}, \tag{6}$$

and

$$\mathrm{TS} = \frac{H}{H + F + M}, \tag{7}$$

where H represents the number of rainfall events successfully predicted, M is the number of the missed events, and F is the number of nonevents erroneously predicted as events. Following Chen et al. (2012) and Brocca et al. (2014), the categorical scores are computed for each point and for different thresholds computed as percentiles of the observed rainfall time series. Therefore, categorical scores are evaluated as a function of rainfall intensity for understanding products' performance in capturing low- to high-rainfall events.

Furthermore, the temporal variability of the products' performance is investigated by estimating the spatial

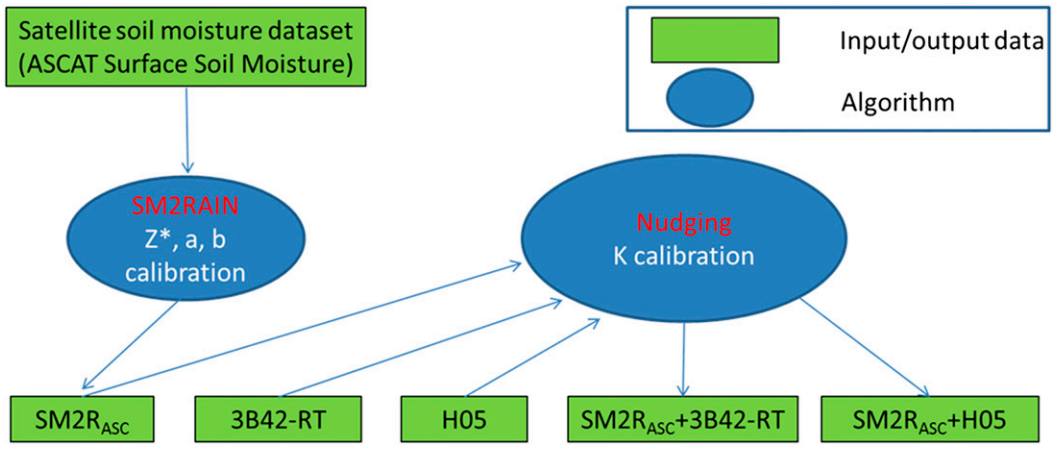

FIG. 1. Flowchart of the analysis method. Variables Z^*, a, and b are the SM2RAIN algorithm parameters [Eq. (3)], SM2R$_{ASC}$ is the rainfall product obtained starting from ASCAT SSM data, 3B42-RT is the TMPA product in real time, H05 is the rainfall product provided by EUMETSAT, SM2R$_{ASC}$+3B42-RT and SM2R$_{ASC}$+H05 are the integrated products, and K is the gain parameter used for the integration [Eq. (4)].

average of the R and the RMSE values on a monthly scale. Specifically, for each month, observed and satellite data for all pixels are appended and the temporal R and RMSE values are finally computed. In this way, the fluctuations at monthly temporal scales can be identified. To investigate the influence of seasonality on products' performance (Ebert et al. 2007; Stampoulis and Anagnostou 2012), the temporal variability at the seasonal scale is also analyzed.

4. Results

In the sequel, five rainfall datasets are evaluated (Fig. 1). Specifically, two state-of-the-art rainfall (H05 and 3B42-RT) and the ASCAT-derived (SM2R$_{ASC}$) products are considered along with the two products obtained from the integration of rainfall and SM data (SM2R$_{ASC}$+H05 and SM2R$_{ASC}$+3B42-RT). The analysis is carried out during the period from 1 January 2010 to 31 December 2013. The calibration phase concerns the period from 1 January 2010 to 31 December 2011, while the validation is from 1 January 2012 to 31 December 2013.

a. Calibration of SM2RAIN and of the integration method

The SM2RAIN parameters are obtained through a spatially distributed pixel-by-pixel calibration. Figure 1 plots a scheme of the SM2RAIN application to SM satellite data and of the analysis steps while Fig. 2 shows the spatial distribution of the obtained parameter values. The Z^* parameter shows the highest values in the two areas in northern Italy that are characterized by

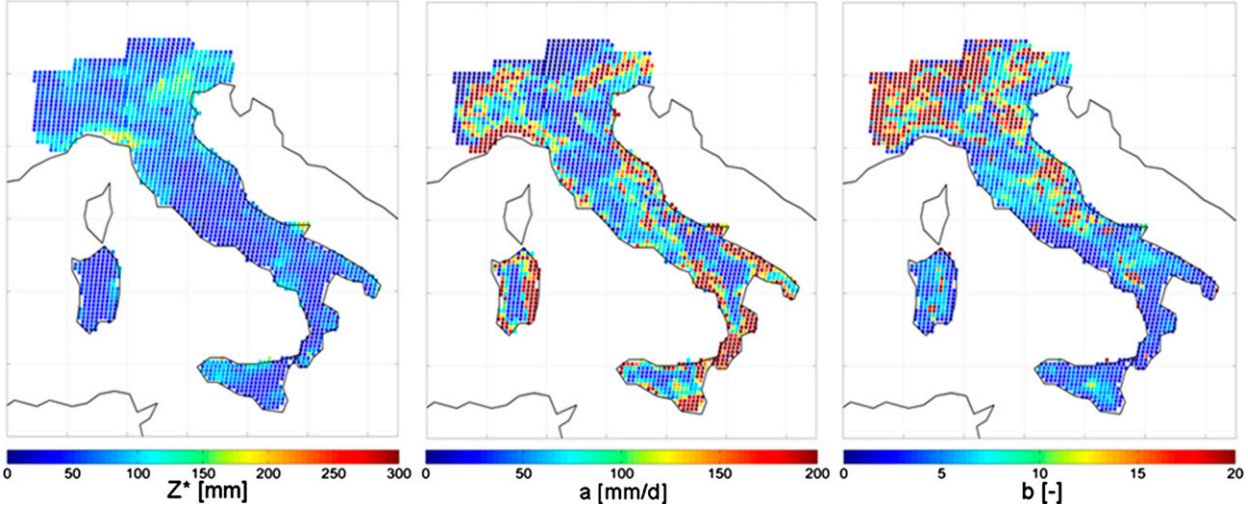

FIG. 2. Spatial distribution of SM2RAIN parameters (left) Z^*, (middle) a, and (right) b.

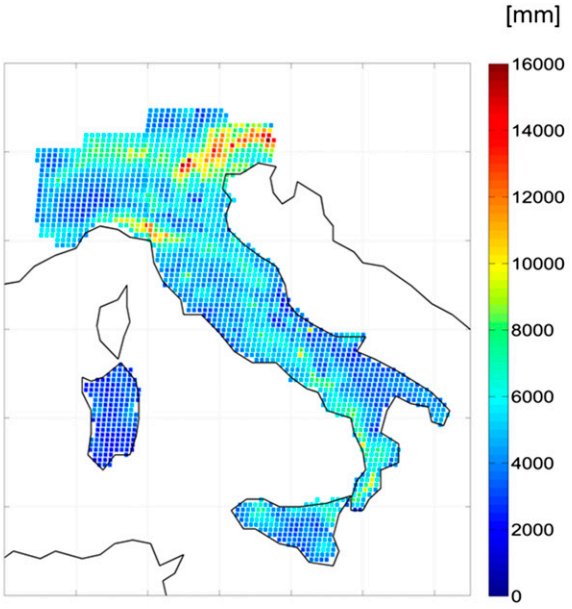

FIG. 3. Cumulated observed rainfall (mm) over the whole analysis period (2010–13).

the highest rainfall regime, as shown in Fig. 3, where the cumulated rainfall over the whole period is plotted. This is in good accordance with Brocca et al. (2014), who obtained increasing Z^* with the rainfall amount in the pixel. The a parameter shows the higher variability throughout the Italian territory, with the highest values along the coastline. This "coast effect" could be traced to the satellite SM retrievals issues at the water–land interface. The b parameter shows the highest values in northern Italy, mainly over the Alps. The variation patterns of the a and b parameters are in agreement with the estimated SM noise map proposed in Bartalis et al. (2008), that is, the higher the uncertainty on SM retrieval, the higher parameter values needed to produce rainfall that contrasts the satellite noise. The SM2RAIN parameters show mean values of 63.62 mm, 94.35 mm day^{-1}, and 8.13 for Z^*, a, and b, respectively. The values of a and b parameters are found to be higher than those obtained by Brocca et al. (2014). This can be explained by the difference in the spatial resolution, 0.125° in this study versus 1° in Brocca et al. (2014). The use of a coarser grid, on which ASCAT SM retrievals were averaged out, allowed the noise to be reduced and, hence, the lower values of the a and b parameters to be obtained. Further studies will be addressed to evaluate the relationship between the SM2RAIN parameters, soil texture, vegetation, and grid resolution using a higher-resolution soil map.

Figure 4 plots the spatial variability of the K parameter (Eq. 4) for the integration of SM2R$_{ASC}$ with H05 and 3B42-RT products. The differences between the distributions of K are due to the different parent

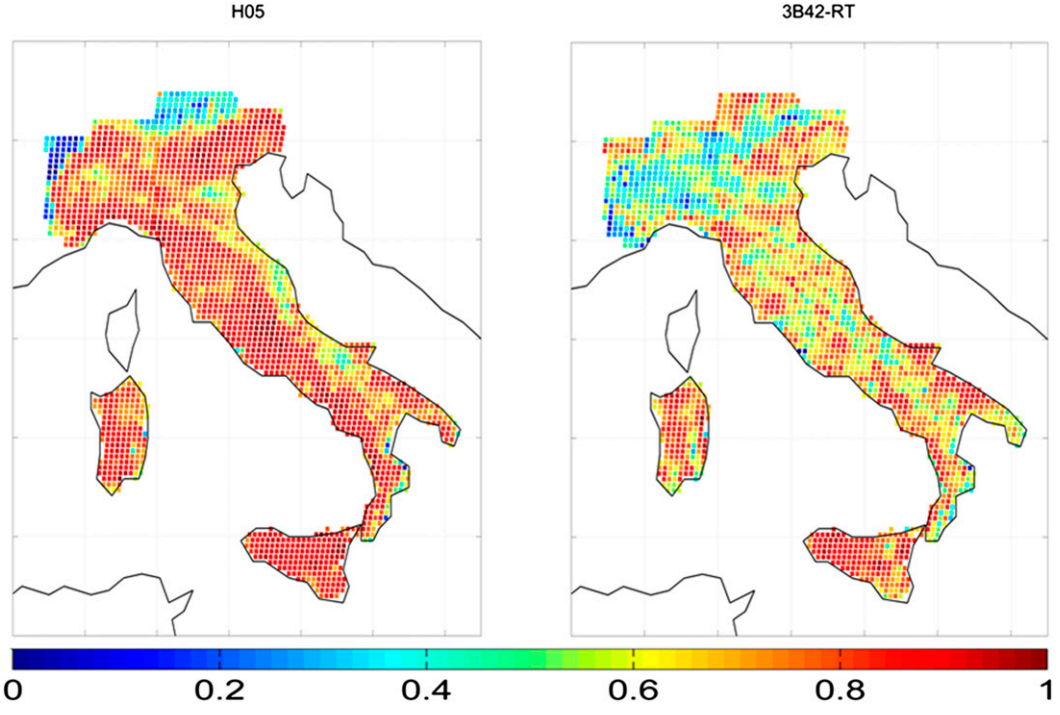

FIG. 4. Spatial distribution of K for (left) H05- and (right) 3B42-RT-integrated products for 5 days of accumulated rainfall; K increases with the weight of the SM2RAIN-derived product with respect to H05 and 3B42-RT products.

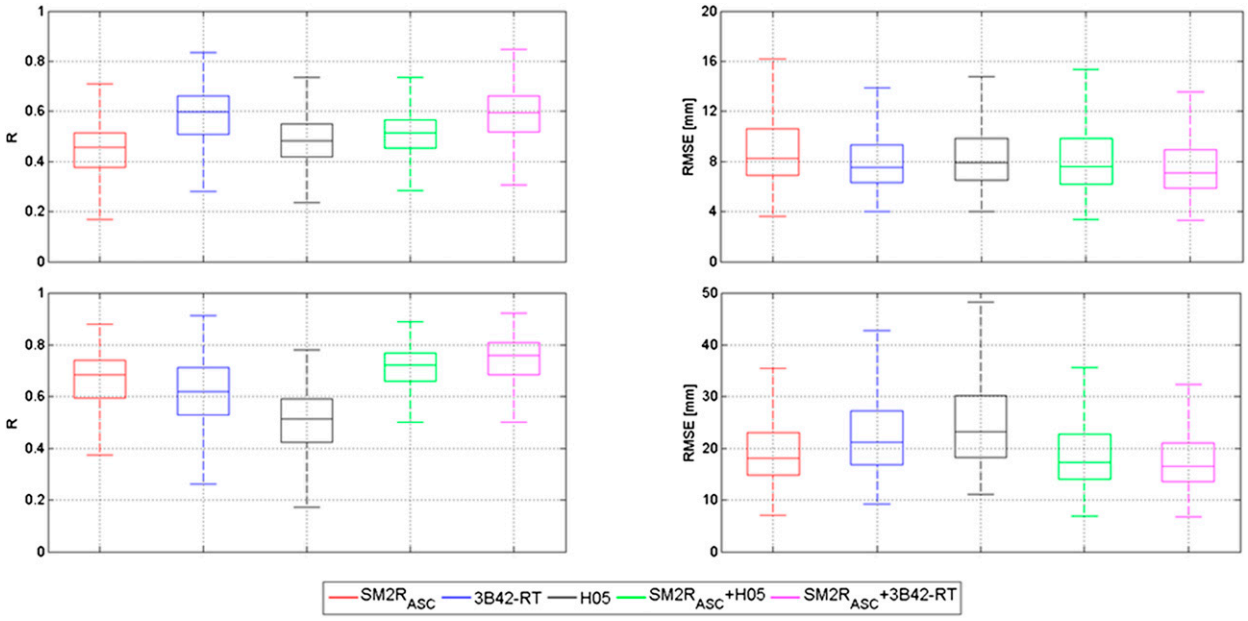

FIG. 5. Boxplot reporting the performance scores [(left) *R* and (right) RMSE] obtained during the calibration period for (top) 1 day and (bottom) 5 days of accumulated rainfall. The box lines represent the 25th, 50th, and 75th percentiles, while the whiskers represent the max and min values.

products performance during the calibration period. The spatial patterns are in agreement with the analyzed products performance obtained during the calibration period (not shown for brevity), with high values of *K* in those areas where $SM2R_{ASC}$ outperforms H05 and 3B42-RT and low values where it provides worse results (e.g., over mountainous areas).

The boxplots in Fig. 5 and the values in Table 2 show the results for the calibration period in terms of *R* and RMSE. As it can be seen, for 1 day of accumulated rainfall, 3B42-RT performs better than $SM2R_{ASC}$ whereas, for 5 days of accumulated rainfall, the $SM2R_{ASC}$ product performs slightly better than 3B42-RT and H05, showing good *R* values and quite low RMSE. The lower performance scores obtained for 1 day of accumulated rainfall depend on several factors: 1) at a daily time step, the noise of ASCAT soil moisture data has a strong impact on the estimated rainfall through SM2RAIN algorithm; 2) the ASCAT soil moisture data are not always available for every day; and 3) the SM2RAIN algorithm is found to perform satisfactorily when applied with a time resolution 3–4 times longer than the resolution of soil moisture data, even when applied with in situ observations (Brocca et al. 2013). Indeed, the change in the storage over a day cannot be related solely to the rainfall, and the use of daily satellite soil moisture observations may lead to errors in daily rainfall estimation. By computing the total rainfall over 5 days, more accurate results can be obtained thanks to an averaging effect. When more accurate and temporally dense satellite soil moisture data are available (e.g., through merging of retrievals from different sensors), more accurate results, even at the daily time scale, are expected.

Concerning the integrated products, results for 1 day of accumulated rainfall show a slight improvement. By way of example, *R* for $SM2R_{ASC}$+H05 shows an increase of 6% with respect to H05, while there is no noticeable difference considering the $SM2R_{ASC}$+3B42-RT product. This is probably due to the lower correlation of $SM2R_{ASC}$ with respect to 3B42-RT. However, in terms of RMSE, there is a reduction of 4% and 6% for both $SM2R_{ASC}$+H05 and $SM2R_{ASC}$+3B42-RT compared to the parent satellite rainfall products. For 5 days of accumulated rainfall, the improvement due to the integration is evident and significant; the integrated products show the highest median *R* values (0.72 and 0.76 for $SM2R_{ASC}$+H05 and $SM2R_{ASC}$+3B42-RT, respectively), with an increase of nearly 41% and 23% compared to the parent products (i.e., H05 and 3B42-RT). In terms of RMSE (for 5 days of accumulated rainfall), the integrated products show a reduction of about 25% and 21% compared to the satellite rainfall datasets with the best results for $SM2R_{ASC}$+3B42-RT (with a median RMSE of 16.60 mm).

b. Products performance in the validation period

After the calibration step, the SM2RAIN algorithm is run on the validation period (2012–13), and the derived

TABLE 2. Median R, median RMSE (mm), and pixels with a significant correlation (p value < 0.01) for each analyzed product (%), during the calibration and validation periods, considering 1 and 5 days of accumulated rainfall (std dev is given in parentheses).

Product	Median R				Median RMSE				Pixels with p value < 0.01			
	Calibration (2010–11)		Validation (2012–13)		Calibration (2010–11)		Validation (2012–13)		Calibration (2010–11)		Validation (2012–13)	
	1 day	5 days	1 day	5 days	1 day	5 days	1 day	5 days	1 day	5 days	1 day	5 days
$SM2R_{ASC}$	0.45 (0.12)	0.68 (0.14)	0.43 (0.13)	0.62 (0.16)	8.27 (3.66)	18.01 (7.95)	8.71 (4.05)	19.94 (10.97)	96%	95%	96%	94%
H05	0.48 (0.09)	0.51 (0.12)	0.50 (0.10)	0.54 (0.11)	7.93 (3.61)	23.22 (11.95)	8.25 (3.68)	22.32 (12.41)	97%	97%	95%	97%
3B42-RT	0.60 (0.11)	0.62 (0.12)	0.57 (0.12)	0.60 (0.13)	7.51 (3.10)	21.16 (10.05)	7.80 (3.44)	21.87 (11.60)	97%	97%	97%	96%
$SM2R_{ASC}$+H05	0.51 (0.09)	0.72 (0.10)	0.51 (0.11)	0.68 (0.11)	7.62 (3.64)	17.36 (8.24)	7.86 (4.03)	18.32 (11.56)	97%	97%	97%	97%
$SM2R_{ASC}$+3B42-RT	0.59 (0.11)	0.76 (0.11)	0.57 (0.12)	0.71 (0.10)	7.06 (3.34)	16.60 (7.71)	7.47 (3.83)	18.13 (10.91)	97%	97%	97%	97%

rainfall dataset is integrated into the 3B42-RT and H05 products by using the distributed parameter values obtained in calibration (2010–11). Then, the comparison between each satellite rainfall product and the observed rainfall data is carried out in terms of R and RMSE for 1 and 5 days of accumulated rainfall. The three categorical scores (POD, FAR, and TS) are only estimated for 5 days of accumulated rainfall.

Table 2 indicates that for 1 and 5 days of accumulated rainfall the validation results are consistent to those obtained in calibration, showing only a little deterioration of the performance scores with respect to the calibration. In particular, significant improvements are obtained for 1 and 5 days of accumulated rainfall of the integrated products with respect to the parent products. The results for 5 days of accumulated rainfall deserve more attention. In this case, the correlation maps in Fig. 6 show good correlation against ground data in all cases. In particular, 3B42-RT results are 1) consistent with those found by Chen et al. (2013), Brocca et al. (2014), and Stampoulis and Anagnostou (2012) at mid-latitude; 2) slightly lower than those of $SM2R_{ASC}$; and 3) better than H05. The integration of the products improves the performance, causing an increase in median R from 0.60 to 0.71 for 3B42-RT and from 0.54 to 0.68 for H05. It is interesting to note that R maps highlight areas where the $SM2R_{ASC}$ product provides less accurate results because of topographic complexity (the Alps and Apennines chains), while both 3B42-RT and H05 products show lower performance in southern Italy. With respect to 3B42-RT performance, Stampoulis and Anagnostou (2012) found similar results. Therefore the integration involves a substantial improvement in the product performance with an increase, during the validation period, in $SM2R_{ASC}$+H05 ($SM2R_{ASC}$+3B42-RT) median R value of about 26% (18%) with respect to the H05 (3B42-RT) product. For assessing the reliability of the analysis in terms of correlation, the percentage of pixels (over 2043) with a p value < 0.01 (significant correlation) have been calculated and reported in Table 2. The high percentage (>94%) of the pixels having a significant correlation confirms the analysis reliability. In particular, the pixels showing a p value > 0.01 are mainly located over the Alps and the Gran Sasso massif for the $SM2R_{ASC}$ product, while H05 and 3B42-RT products show pixels with a p value > 0.01 over southern Italy and the mountainous regions, as might be expected by looking the correlation maps (Fig. 6).

In Fig. 7, the RMSE maps for the validation period are shown. Median values of 19.94, 21.87, 22.32, 18.32, and 18.13 mm are obtained for $SM2R_{ASC}$, 3B42-RT, H05, $SM2R_{ASC}$+H05, and $SM2R_{ASC}$+3B42-RT, respectively.

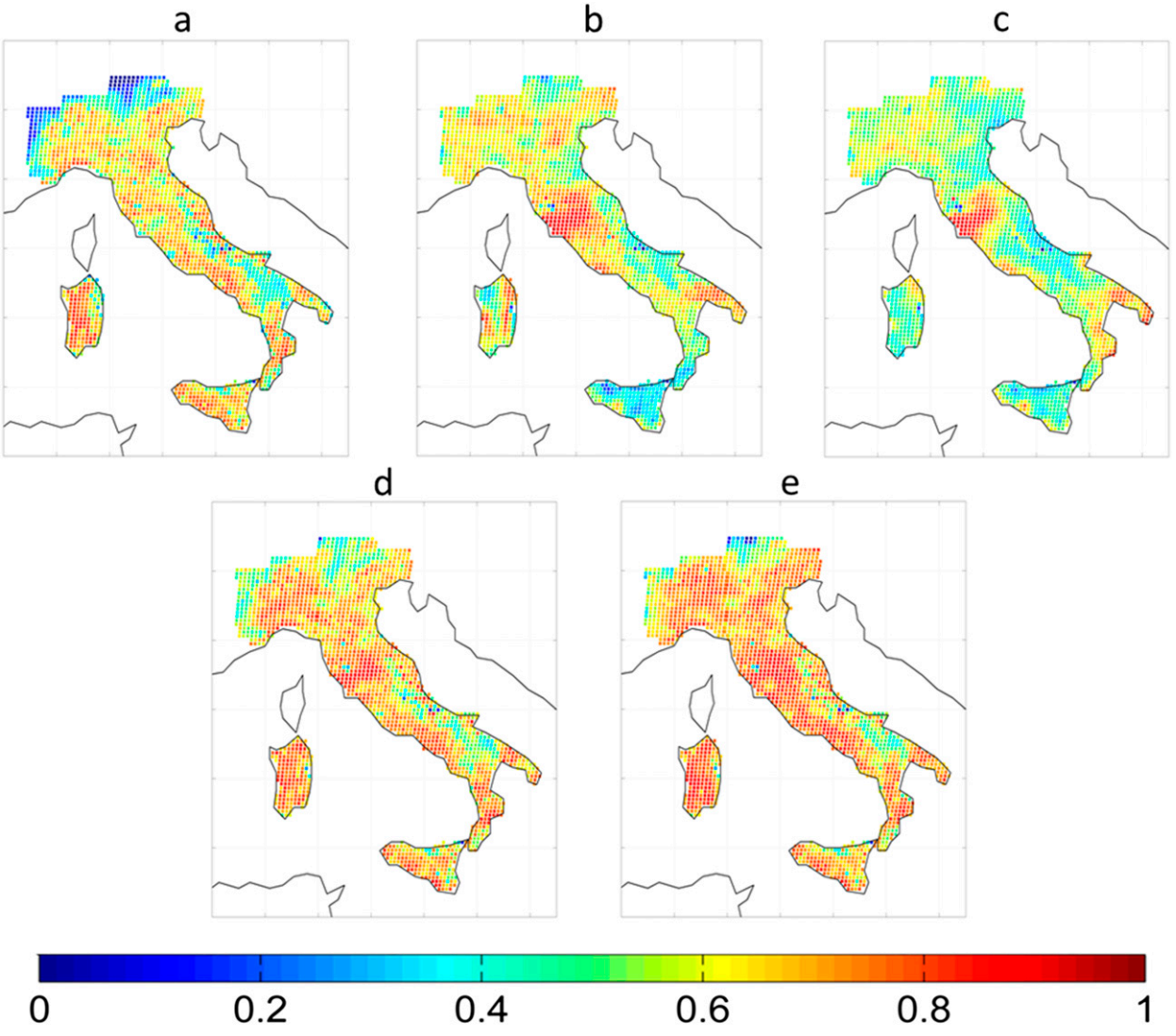

FIG. 6. Maps of R for 5 days of accumulated rainfall for (a) $SM2R_{ASC}$ (median $R = 0.62$), (b) 3B42-RT (median $R = 0.6$), (c) H05 (median $R = 0.53$), (d) $SM2R_{ASC}$+H05 (median $R = 0.68$), and (e) $SM2R_{ASC}$+3B42-RT (median $R = 0.71$) during the validation period (2012–13).

The high error values displayed in two areas in northern Italy are related to larger rainfall amounts (see Fig. 3). In terms of RMSE, a reduction of about 18% and 17% can be seen for $SM2R_{ASC}$+H05 and $SM2R_{ASC}$+3B42-RT, respectively.

A sensitivity analysis has been also carried out in order to investigate the sensitivity of the results on the estimated K values (not shown for brevity). First, the use of spatially uniform K values is analyzed by computing the performance of the integrated products with K varying between 0 and 1 (a step of 0.1). If compared with the spatially distributed calibration (see Table 2), the performance is slightly better in terms of median R values that are equal to 0.70 (0.74) for $SM2R_{ASC}$+H05 ($SM2R_{ASC}$+3B42-RT) and worse in terms of median RMSE that are equal to 25.6 mm (26.4 mm) for $SM2R_{ASC}$+H05 ($SM2R_{ASC}$+3B42-RT). The spatially constant K value that provides the best results is equal to 0.6 (0.7) for $SM2R_{ASC}$+H05 ($SM2R_{ASC}$+3B42-RT), close to the median values obtained in the spatially distributed calibration (0.79 and 0.68 for $SM2R_{ASC}$+H05 and $SM2R_{ASC}$+3B42-RT, respectively). Moreover, an additional analysis is carried out by recalibrating, pixel by pixel, the K values in the validation period. For this experiment, the median R values (RMSE values) are equal to 0.69 and 0.73 (90 and 90) for $SM2R_{ASC}$+H05 and $SM2R_{ASC}$+3B42-RT, respectively. Therefore, the performance of the integrated products is not sensitive to the

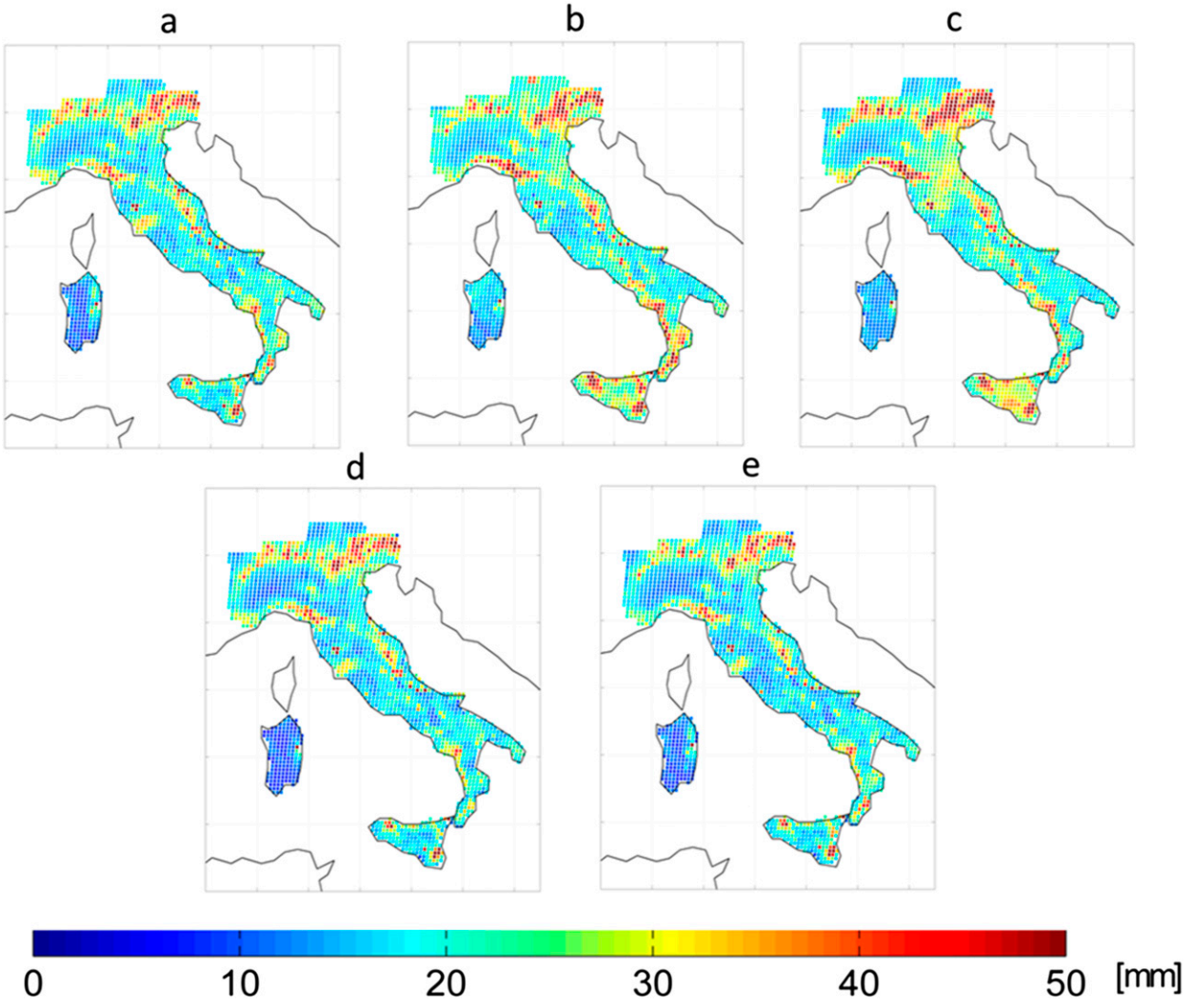

FIG. 7. Maps of RMSE for 5 days of accumulated rainfall for (a) $SM2R_{ASC}$ (median RMSE = 19.94 mm), (b) 3B42-RT (median RMSE = 21.87 mm), (c) H05 (median RMSE = 22.32 mm), (d) $SM2R_{ASC}$+H05 (median RMSE = 18.32 mm), and (e) $SM2R_{ASC}$+3B42-RT (median RMSE = 18.13 mm) during the validation period (2012–13).

K values used for the integration, as could be expected, thus highlighting the robustness of the overall procedure. However, more complex assimilation schemes, as well as more frequent recalibrations, will be analyzed in future studies in order to determine the best integration procedure.

c. Categorical score assessment

The POD, FAR, and TS values are computed by considering percentile thresholds based on the observed rainfall distribution at each pixel. The results for 5 days of accumulated rainfall are displayed in Fig. 8. The figure shows that the 3B42-RT product has the lowest FAR and POD, probably because of the difficulty in estimating light rainfall, while H05 has the highest values of POD, mainly when considering the first percentiles. The integrated products generally outperform the parent products, providing a small reduction of FAR for higher percentiles (>70th percentile) and an increase in the detection of rainfall events (i.e., POD) for nearly all the considered thresholds. Consequently, higher TS values are obtained from the integrated products for >50th percentiles, that is, for higher rainfall rates that are more of interest for hydrological applications addressing flood and landslide prediction.

d. Spatial analysis of the rainfall products

The analysis of the products' capability of reproducing rainfall spatial variability is carried out by considering

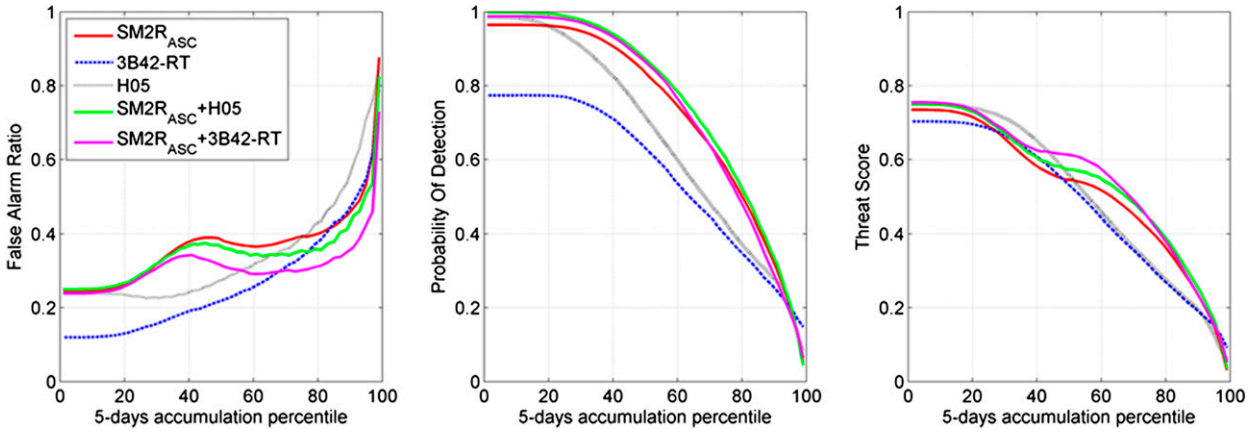

FIG. 8. Spatial averages of categorical metrics, computed for 5 days of accumulated rainfall, for the analyzed rainfall products ($SM2R_{ASC}$, 3B42-RT, H05, $SM2R_{ASC}$+H05, and $SM2R_{ASC}$+3B42-RT) in the validation period (2012–13): (left) FAR, (middle) POD, and (right) TS for a 5-day rainfall accumulation threshold. An event is defined as a 5-day rainfall accumulation that exceeds a given percentile threshold of all 5-day accumulations observed for a given pixel over the analyzed period.

the entire analysis period and 5 days of accumulated rainfall. For each day of the analysis period, the *R* and RMSE values are computed by comparing the observed and satellite rainfall maps. The analyzed products show mean *R* values of 0.52, 0.43, 0.52, 0.58, and 0.55 for $SM2R_{ASC}$, 3B42-RT, H05, $SM2R_{ASC}$+3B42-RT, and $SM2R_{ASC}$+H05, respectively. In terms of RMSE, mean values of 20.34, 22.28, 22.84, 18.60, and 19.32 mm are obtained for $SM2R_{ASC}$, 3B42-RT, H05, $SM2R_{ASC}$+3B42-RT, and $SM2R_{ASC}$+H05, respectively. These results are found to be comparable with those obtained with the temporal analysis, with an improvement in the performance obtained for the integrated products that are thus capable of better reproducing both the temporal and spatial rainfall variability.

e. Temporal variability of the product performance

The temporal variability of the product performance is investigated by estimating *R* and RMSE values on a monthly scale in order to evaluate their trends during the entire period (2010–13). Specifically, for each month, the temporal *R* and RMSE values are computed by appending the time series of each pixel. Figure 9 shows a general agreement between the analyzed products: $SM2R_{ASC}$, $SM2R_{ASC}$+3B42-RT, and $SM2R_{ASC}$+H05 show *R* values between 0.38 and 0.82. The other two products show more pronounced fluctuations in *R* value, between 0.13 and 0.75. All products show poor performance values during the winter months (Tian et al. 2009). In terms of RMSE, all the considered rainfall products have a similar pattern, with higher values (up to 50 mm) during winter months and lower values during summer months (due to the RMSE dependency on rainfall amount).

The temporal analysis is also carried out by considering each individual season, that is, the entire analysis period is split into four different time ranges according to season. For spring the months of March–May (MAM) are considered, for summer June–August (JJA), for fall September–November (SON), and for winter December–February (DJF). For each period POD, FAR, and TS values are calculated (considering 5 days of accumulated rainfall) and averaged in space (over the 2043 grid points) and in time (every performance score presents four values, one for each year of the analysis period). In this way, one value per season is obtained. In Fig. 10, the POD and FAR values are plotted for each season, considering the 10th and 90th percentile thresholds. Specifically, in Fig. 10, the closer a point is to the lower-right corner of the plot, the better the performance is. By contrast, the proximity of a point to the upper-left corner suggests worse performance. On this basis, a downward and/or rightward variation implies an improvement. In terms of TS, Fig. 10 highlights that all the rainfall products perform better during the JJA and SON period than during MAM and DJF, mainly for the 90th percentile. The parent products (i.e., H05 and 3B42-RT) show the lowest performance during the MAM and DJF periods, probably because of the tendency of these products to underestimate light rainfall (Kidd and Levizzani 2011).

To visualize the temporal variability of rainfall products, two representative time series are reported in Fig. 11. Specifically, two pixels are selected throughout the study area, in order to show good and bad integration results in the calibration and validation period. The pixels are chosen by considering the RMSE difference between the parent and the integrated products for

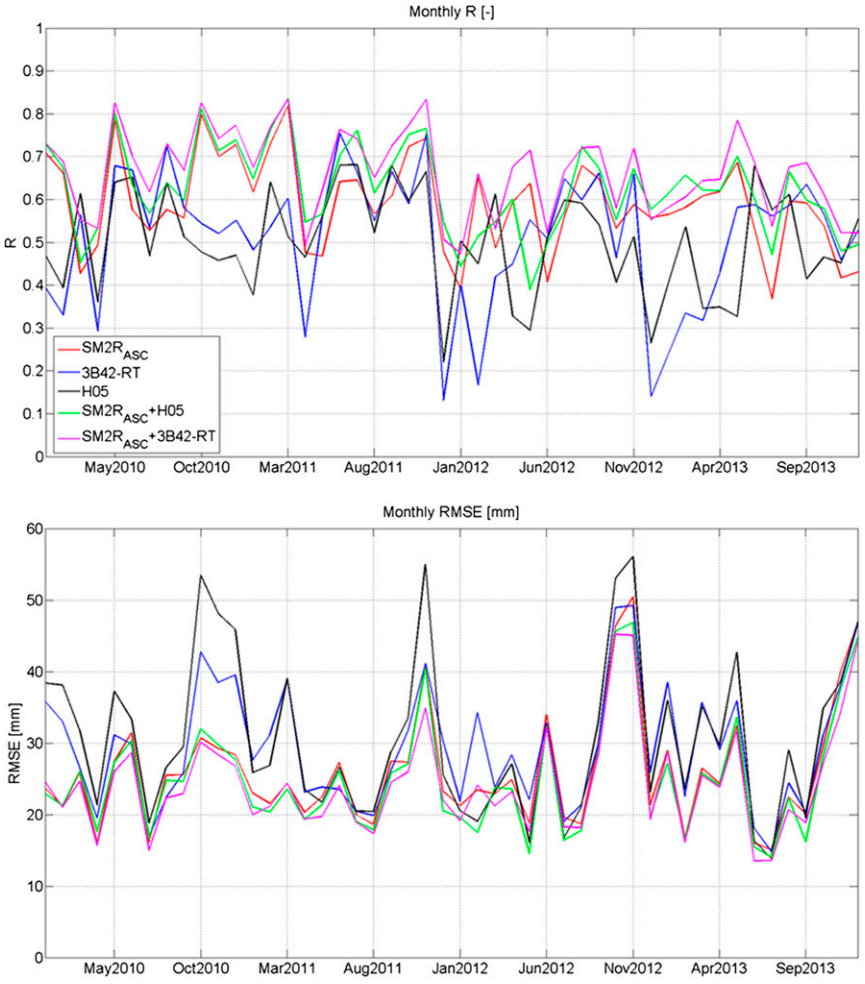

FIG. 9. Monthly (top) *R* and (bottom) RMSE values for 5 days of accumulated rainfall for each analyzed product.

5 days of accumulated rainfall during the calibration period. Figures 11a and 11b show the bad integration results with RMSE values equal to 25.59 and 34.93 mm for the $SM2R_{ASC}$+3B42-RT and $SMR2_{ASC}$+H05 products, respectively, while the parent products (i.e., 3B42-RT and H05) provide RMSE values equal to 26.08 and 37.43 mm. As can be seen from the plot, the integrated products' time series are characterized by a general underestimation during both the calibration and validation periods. The pixel is chosen over a mountainous area where the parent products are affected by many factors, such as the presence of snow/frozen soil and complex topography, and they do not provide good performance separately. As a result, their integration does not yield a satisfactory score. In contrast, Figs. 11c and 11d plot the time series for the good integration results. The RMSE values for the integrated products are 21.26 and 21.30 mm, for $SM2R_{ASC}$+3B42-RT and $SMR2_{ASC}$+H05, respectively, while the parent products show nearly double RMSE values equal to 41.24 and 46.91 mm. Figures 11c and 11d show a general agreement between the observed and the integrated products, confirming the capability of the SM2RAIN method to correctly estimate rainfall and the usefulness of the proposed integration procedure that allowed for a more reliable rainfall dataset by partially overcoming the satellite issues related to light rainfall estimation. The presented case studies highlight the benefits due to the integration in different rainfall regimes.

5. Conclusions

In this paper, an integration of satellite rainfall and soil moisture data is presented. The 3B42-RT and H05 rainfall products are integrated with ASCAT-derived rainfall data, through the application of the SM2RAIN

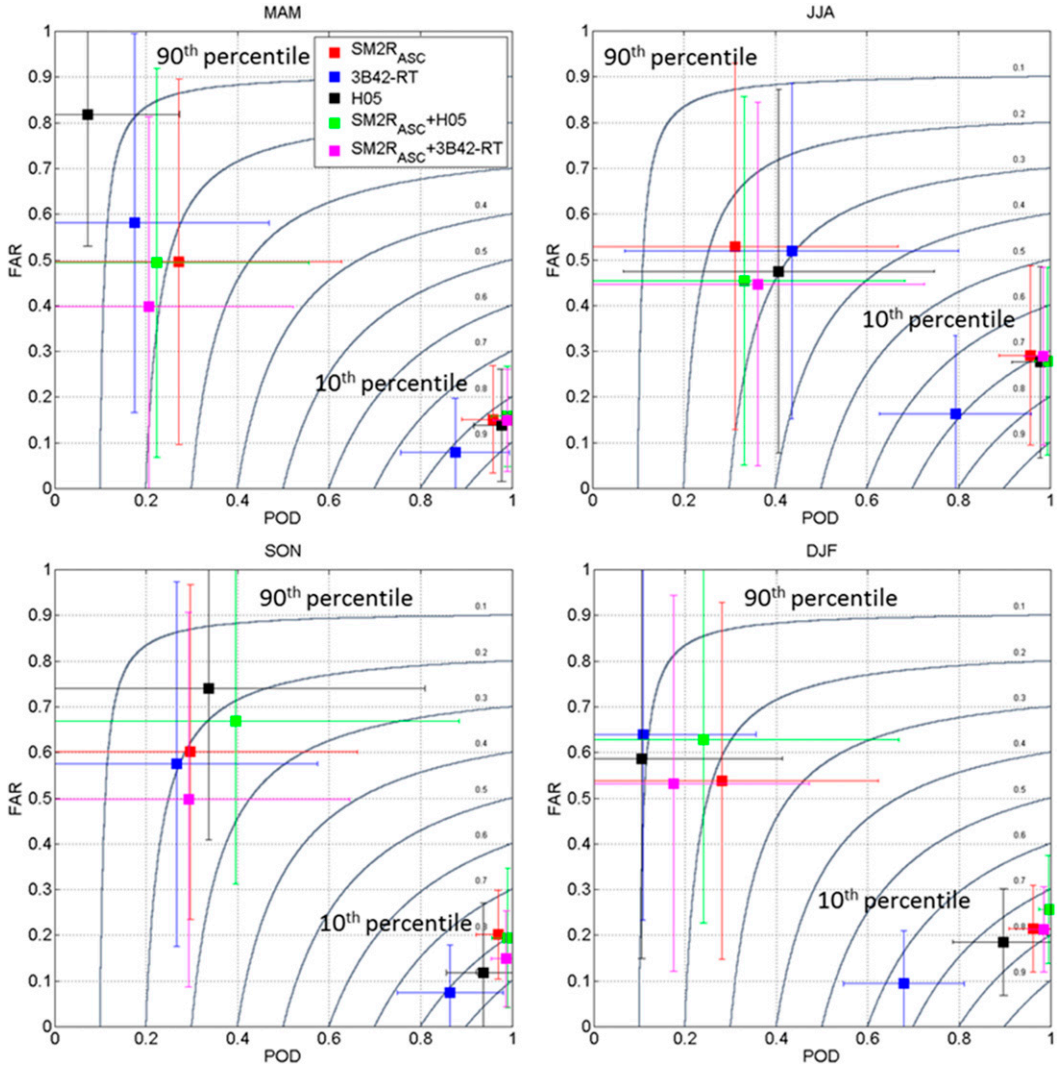

FIG. 10. POD vs FAR plot for each seasonal period considering 5 days of accumulated rainfall. The gray lines indicate TS values, the horizontal bars represent the std dev of POD, and the vertical bars represent the std dev of FAR for each analyzed percentile.

algorithm, in order to improve the rainfall products' accuracy and reliability. To assess benefits related to the integration, various performance metrics are used to validate the proposed method, evaluating both their spatial and temporal variability against observed rainfall data over the Italian territory.

All the analyzed rainfall products have proven to be in agreement with the observed dataset, showing quite high correlation and low RMSE values. In particular, the SM2RAIN method satisfactorily reproduces rainfall patterns and amounts. The integration analysis has shown an improvement in the performance of the parent products. In particular, the $SM2R_{ASC}$+H05 and $SM2R_{ASC}$+3B42-RT products show the highest correlation values and the lowest RMSE values, considering 5 days of accumulated rainfall. The integration determines an increase in the median R values by up to 41% (23%) for $SM2R_{ASC}$+H05 ($SM2R_{ASC}$+3B42-RT), with respect to the parent product, during the calibration period and by up to 26% (18%) for $SM2R_{ASC}$+H05 ($SM2R_{ASC}$+3B42-RT), during the validation period. With respect to the RMSE, the integration provides a decrease of the median value up to 25% (21%) during the calibration period and up to 18% (17%) during the validation period for $SM2R_{ASC}$+H05 ($SM2R_{ASC}$+3B42-RT). In terms of categorical scores, a reduction in the FAR (for high rainfall rates) and an increase in the POD values of the parent products can be seen. All the analyzed

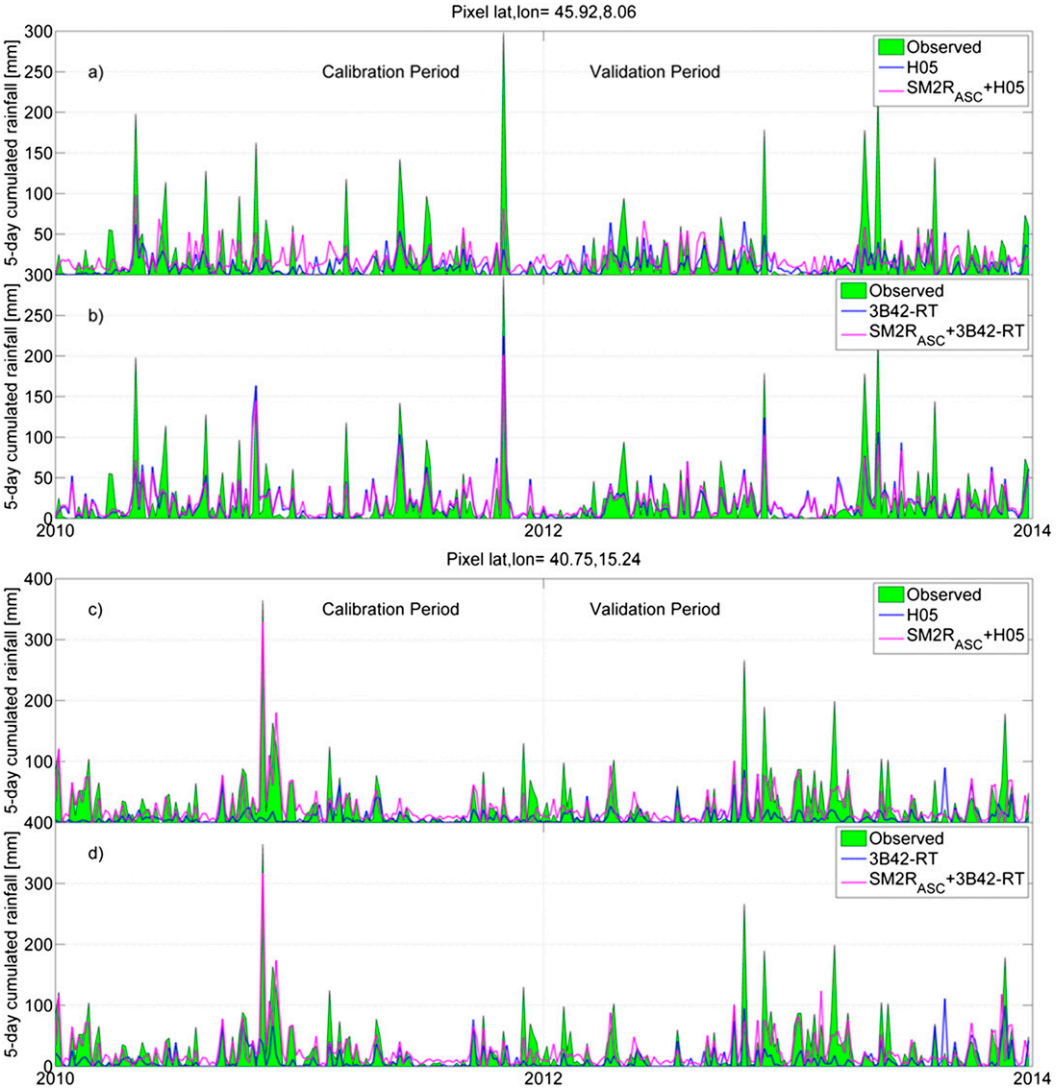

FIG. 11. Time series for the two selected pixels throughout the study area, showing (a),(b) bad integration results and (c),(d) good results in terms of the variation in RMSE after the integration. (a) Results for H05 and $SM2R_{ASC}$+H05 (RMSE values of 37.43 and 34.93 mm, respectively) and (b) results for 3B42-RT and $SM2R_{ASC}$+3B42-RT (RMSE values of 26.08 and 25.59 mm, respectively) for 5 days of accumulated rainfall. (c) Results for H05 and $SM2R_{ASC}$+H05 (RMSE values of 46.91 and 21.30 mm, respectively) and (d) results for 3B42-RT and $SM2R_{ASC}$+3B42-RT (RMSE values of 41.24 and 21.26 mm, respectively).

products have also proven to satisfactorily reproduce the observed rainfall spatial variability with mean *R* values of 0.52, 0.43, 0.52, 0.58, and 0.55 for $SM2R_{ASC}$, 3B42-RT, H05, $SM2R_{ASC}$+3B42-RT, and $SM2R_{ASC}$+H05, respectively. The temporal analysis has confirmed the satellite products' dependency on the season. Better performances are obtained during the warm period for all the analyzed products, whereas 3B42-RT, H05, and $SM2R_{ASC}$ show lower *R* values during DJF and higher values during the SON period.

By performing the analysis over a 4-yr period, these results are also useful for giving indications of the capability of the analyzed rainfall products for hydrological applications. Specifically, this is the first study performing the validation of 3B42-RT and H05 products over Italy with a high-quality observational dataset.

To summarize, satellite soil moisture data are found to be a way of improving satellite rainfall products. The proposed procedure is going to be further enhanced by using more advanced data-assimilation procedures for taking the temporal variability of product errors into account. Finally, as H05, 3B42-RT, and ASCAT satellite data are operational products, the integration can be easily applied in near–real time. This feature makes this

integration method feasible to be applied also for Civil Protection Service early warning systems for addressing the prediction and mitigation of natural hazards such as floods and landslides.

Acknowledgments. The authors gratefully acknowledge support from the ESA Climate Change Initiative (CCI) (ESA/ESRIN Contract 4000104814/11/I-NB; www.esa-soilmoisture-cci.org) and EUMETSAT through the "Satellite Application Facility on Support to Operational Hydrology and Water Management (H-SAF)" (http://hsaf.meteoam.it/). This work is supported by the Italian Civil Protection Department. The authors acknowledge the Italian Civil Protection Department for providing the data from the national meteorological observation networks.

REFERENCES

Bartalis, Z., V. Naeimi, S. Hasenauer, and W. Wagner, 2008: ASCAT soil moisture product handbook. ASCAT Soil Moisture Rep. 15, Institute of Photogrammetry and Remote Sensing, Vienna University of Technology, Vienna, Austria, 22 pp.

Brocca, L., F. Melone, T. Moramarco, and W. Wagner, 2013: A new method for rainfall estimation through soil moisture observations. *Geophys. Res. Lett.,* **40,** 853–858, doi:10.1002/grl.50173.

——, and Coauthors, 2014: Soil as a natural rain gauge: Estimating rainfall from global satellite soil moisture data. *J. Geophys. Res. Atmos.,* **119,** 5128–5141, doi:10.1002/2014JD021489.

Chen, F., W. T. Crow, and T. H. Holmes, 2012: Improving long-term, retrospective precipitation datasets using satellite-based surface soil moisture retrievals and the soil moisture analysis rainfall tool. *J. Appl. Remote Sens.,* **6,** 063604, doi:10.1117/1.JRS.6.063604.

Chen, S., and Coauthors, 2013: Evaluation of the successive V6 and V7 TRMM multisatellite precipitation analysis over the continental United States. *Water Resour. Res.,* **49,** 8174–8186, doi:10.1002/2012WR012795.

Ciabatta, L., L. Brocca, T. Moramarco, and W. Wagner, 2015: Comparison of different satellite rainfall products over the Italian territory. *Engineering Geology for Society and Territory,* Vol. 3, 623–626, doi:10.1007/978-3-319-09054-2_124.

Crow, W. T., G. J. Huffman, R. Bindlish, and T. J. Jackson, 2009: Improving satellite-based rainfall accumulation estimates using spaceborne surface soil moisture retrievals. *J. Hydrometeor.,* **10,** 199–212, doi:10.1175/2008JHM986.1.

Dinku, T., P. Ceccato, E. Grover-Kopec, M. Lemma, S. J. Connor, and C. F. Ropelewsky, 2007: Validation of satellite rainfall products over East Africa's complex topography. *Int. J. Remote Sens.,* **28,** 1503–1526, doi:10.1080/01431160600954688.

Ebert, E. E., J. E. Janowiak, and C. Kidd, 2007: Comparison of near-real-time precipitation estimates from satellite observations and numerical models. *Bull. Amer. Meteor. Soc.,* **88,** 47–64, doi:10.1175/BAMS-88-1-47.

Famiglietti, J. S., and E. F. Wood, 1994: Multiscale modeling of spatially variable water and energy balance processes. *Water Resour. Res.,* **30,** 3061–3078, doi:10.1029/94WR01498.

Huffman, G. J., and Coauthors, 2007: The TRMM Multisatellite Precipitation Analysis: Quasi-global, multi-year, combined-sensor precipitation estimates at fine scale. *J. Hydrometeor.,* **8,** 38–55, doi:10.1175/JHM560.1.

Jackson, T. J., M. H. Cosh, R. Bindlish, and J. Du, 2007: Validation of AMSR-E soil moisture algorithms with ground based networks. *Proc. International Geoscience and Remote Sensing Symposium 2007,* Barcelona, Spain, IEEE, 1181–1184, doi:10.1109/IGARSS.2007.4423015.

Kidd, C., and V. Levizzani, 2011: Status of satellite precipitation retrievals. *Hydrol. Earth Syst. Sci.,* **15,** 1109–1116, doi:10.5194/hess-15-1109-2011.

——, P. Bauer, J. Turk, G. J. Huffman, R. Joyce, K. L. Hsu, and D. Braithwaite, 2012: Intercomparison of high-resolution precipitation products over the northwest Europe. *J. Hydrometeor.,* **13,** 67–83, doi:10.1175/JHM-D-11-042.1.

Kucera, P. A., E. E. Ebert, F. J. Turk, V. Levizzani, D. Kirschbaum, F. J. Tapiador, A. Loew, and M. Borsche, 2013: Precipitation from space: Advancing Earth system science. *Bull. Amer. Meteor. Soc.,* **94,** 365–375, doi:10.1175/BAMS-D-11-00171.1.

Massari, C., L. Brocca, T. Moramarco, Y. Tramblay, and J.-F. Didon Lescot, 2014: Potential of soil moisture observations in flood modelling: Estimating initial conditions and correcting rainfall. *Adv. Water Resour.,* **74,** 44–53, doi:10.1016/j.advwatres.2014.08.004.

Mugnai, A., and Coauthors, 2013: Precipitation products from the hydrology SAF. *Nat. Hazards Earth Syst. Sci.,* **13,** 1959–1981, doi:10.5194/nhess-13-1959-2013.

Pellarin, T., S. Louvet, C. Gruhier, G. Quantin, and C. Legout, 2013: A simple and effective method for correcting soil moisture and precipitation estimates using AMSR-E measurements. *Remote Sens. Environ.,* **136,** 28–36, doi:10.1016/j.rse.2013.04.011.

Pignone, F., N. Rebora, F. Silvestro, and F. Castelli, 2010: GRISO–Rain. Operational Agreement 778/2009 DPC-CIMA, Year-1 Activity Rep. 272/2010, CIMA Research Foundation, Savona, Italy, 353 pp.

Puca, S., and Coauthors, 2014: The validation service of the hydrological SAF geostationary and polar satellite precipitation products. *Nat. Hazards Earth Syst. Sci.,* **14,** 871–889, doi:10.5194/nhess-14-871-2014.

Rudolf, B., and U. Schneider, 2005: Calculation of gridded precipitation data for the global land-surface using in-situ gauge observations. *Proc. Second Workshop Int. Precipitation Working Group,* Monterey, CA, NRL/EUMETSAT, 231–247.

Stampoulis, D., and E. N. Anagnostou, 2012: Evaluation of global satellite rainfall products over continental Europe. *J. Hydrometeor.,* **13,** 588–603, doi:10.1175/JHM-D-11-086.1.

Tian, Y., and Coauthors, 2009: Component analysis of errors in satellite-based precipitation estimates. *J. Geophys. Res.,* **114,** D24101, doi:10.1029/2009JD011949.

Wagner, W., and Coauthors, 2013: The ASCAT soil moisture product: A review of its specifications, validation results, and emerging applications. *Meteor. Z.,* **22,** 5–33, doi:10.1127/0941-2948/2013/0399.